Hub GABA neurons mediate gamma-frequency oscillations at ictal-like event onset in the immature hippocampus

PP Quilichini, M Le Van Quyen, A Ivanov, DA Turner, A Carabalona, H Gozlan, M Esclapez, C Bernard

Supplemental Data

Figure S1. The CA1 region contains the sufficient circuitry to generate stable fast oscillations, which depend upon $GABA_A$ receptors activation.

(A1) Large network discharges (ictal-like activities; ILEs) started to occur twenty minutes following the perfusion of low Mg^{2+}-containing ACSF and showed a stable frequency (every six minutes) during long-term (> 2 h) recordings, as reported previously (Quilichini et al., 2002).

(A2) The first ILE is shown on an expanded time-scale.

(A3) Time-frequency (TF) content analysis revealed the presence of GFOs at ILE onset (ILE1). GFOs were specific to ILEs onset, as they were not present elsewhere during or between ILEs, including during isolated interictal-like events. (TFe: TF energy).

(A4) GFOs also displayed remarkable stability between the beginning and the end of the recording sessions. The GFOs at the onset of the 6^{th} (ILE6) and 15^{th} (ILE15) ILEs were very similar to the GFOs recorded at the onset of the first one.

(B1) Surgical removal of the septum did not affect the occurrence of GFOs in the CA1 region.

(B2) ILEs and GFOs were still present in the isolated CA1 region, demonstrating that this region retains the minimum circuitry to generate GFOs at ILE onset.

(C) The expression of GFOs was strongly reduced at ILE onset by the $GABA_A$ receptor antagonist bicuculline (10 µM; 24±6%, n=26 ILEs, $p<0.05$) but not by the AMPA/kainate receptor antagonist NBQX (10 µM; n=20 ILEs, $p>0.05$), indicating that GFOs depend upon $GABA_A$ receptor activation, not AMPA receptors. Neither the mean frequency (C1) nor the number (C2) of GFOs were affected by NBQX, suggesting that phasic AMPA/KA synaptic excitation by pyramidal cells is not required for their generation.

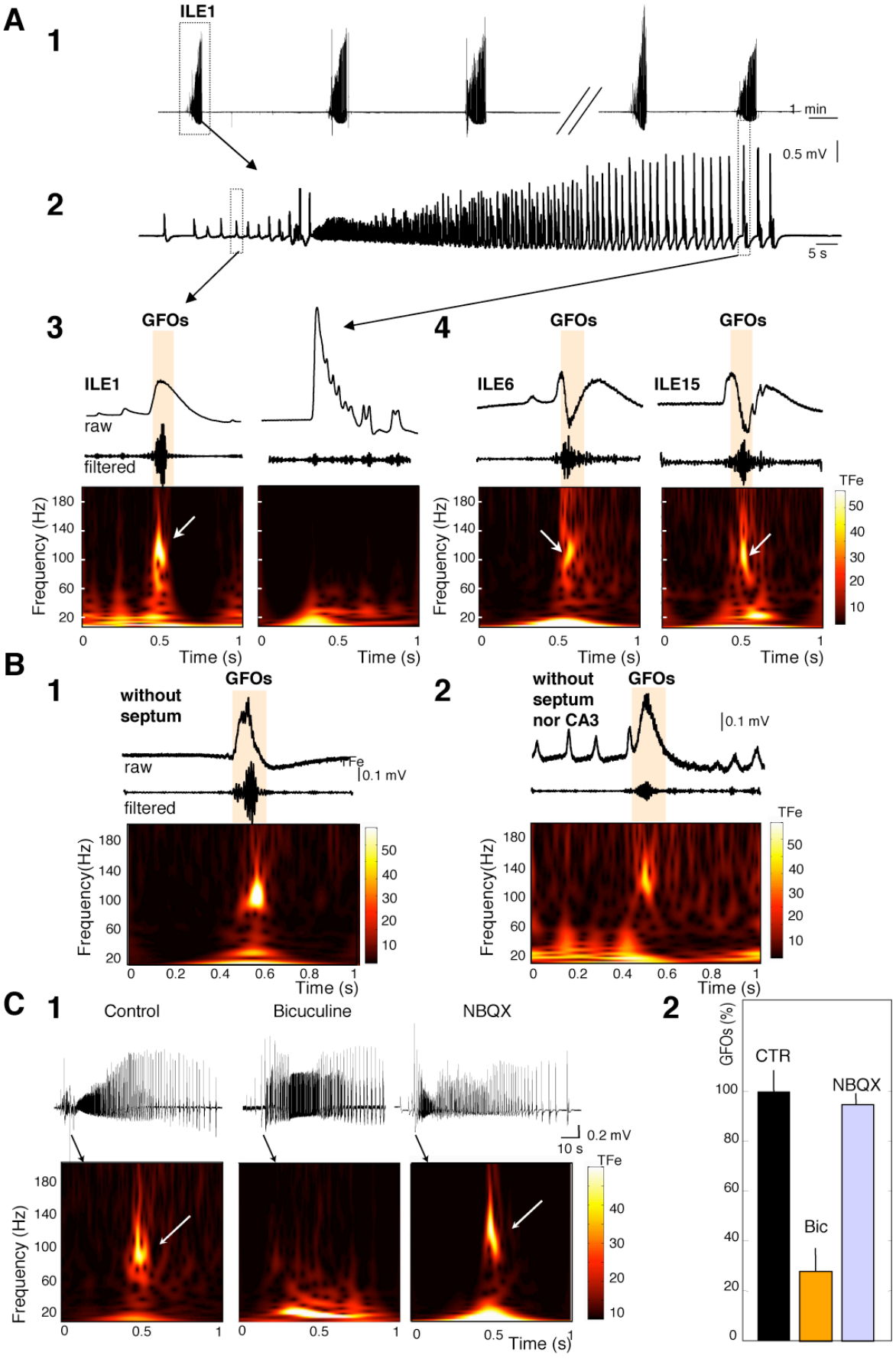
A
1
ILE1
1 min
0.5 mV
2
5 s
3
GFOs
ILE1
raw
filtered
Frequency (Hz)
180
140
100
60
20
0
0.5
1
Time (s)
4
GFOs
GFOs
ILE6
ILE15
TFe
50
40
30
20
10
B
1
without septum
GFOs
raw
filtered
TFe
0.1 mV
Frequency(Hz)
Time (s)
2
without septum nor CA3
GFOs
0.1 mV
TFe
C
1
Control
Bicuculine
NBQX
0.2 mV
10 s
TFe
Frequency (Hz)
Time (s)
2
GFOs (%)
CTR
NBQX
Bic
100
80
60
40
20
0

Figure S2. Examples of morphologically identified hippocampal neurons.

(A) CA3 pyramidal cell recorded at P6. Arrowheads indicate the axon with its ramifications in CA1 (Schaffer collateral) and, locally, in CA3 (associational pathway).

(B) CA1 pyramidal cell recorded at P5.

(C) CA1 O-LM interneuron recorded at P5. Arrowheads indicate the axon with its ramifications in the *stratum lacunosum moleculare*.

(D) CA1 *stratum oriens* perisomatic interneuron (putative basket cell) recorded at P6. The axon (arrowheads) ramifies extensively in *stratum pyramidale*.

(E) CA1 backprojecting interneuron recorded at P6.

Thirty-six biocytin labeled cells were identified as interneurons based on morphological features distinguishing them from pyramidal cells. Fourteen neurons could be assigned to a specific cell type. Incomplete axon filling of the remaining ones prevented a complete identification. This morphological analysis includes the neurons recorded in cell attached condition and voltage clamp during GFOs. A similar morphological analysis was performed following the experiments designed to determine the connectivity pattern of HS cells (see also Figure S3A-B), as well as the resting membrane potential and the chloride reversal potential in interneurons (see also Figure S3C-D).

O. *stratum oriens*, P: *stratum pyramidale*, R: *stratum radiatum*, LM: *stratum lacunosum moleculare*. Scale bars: A, B, C 50 *μ*m; D 25 *μ*m.

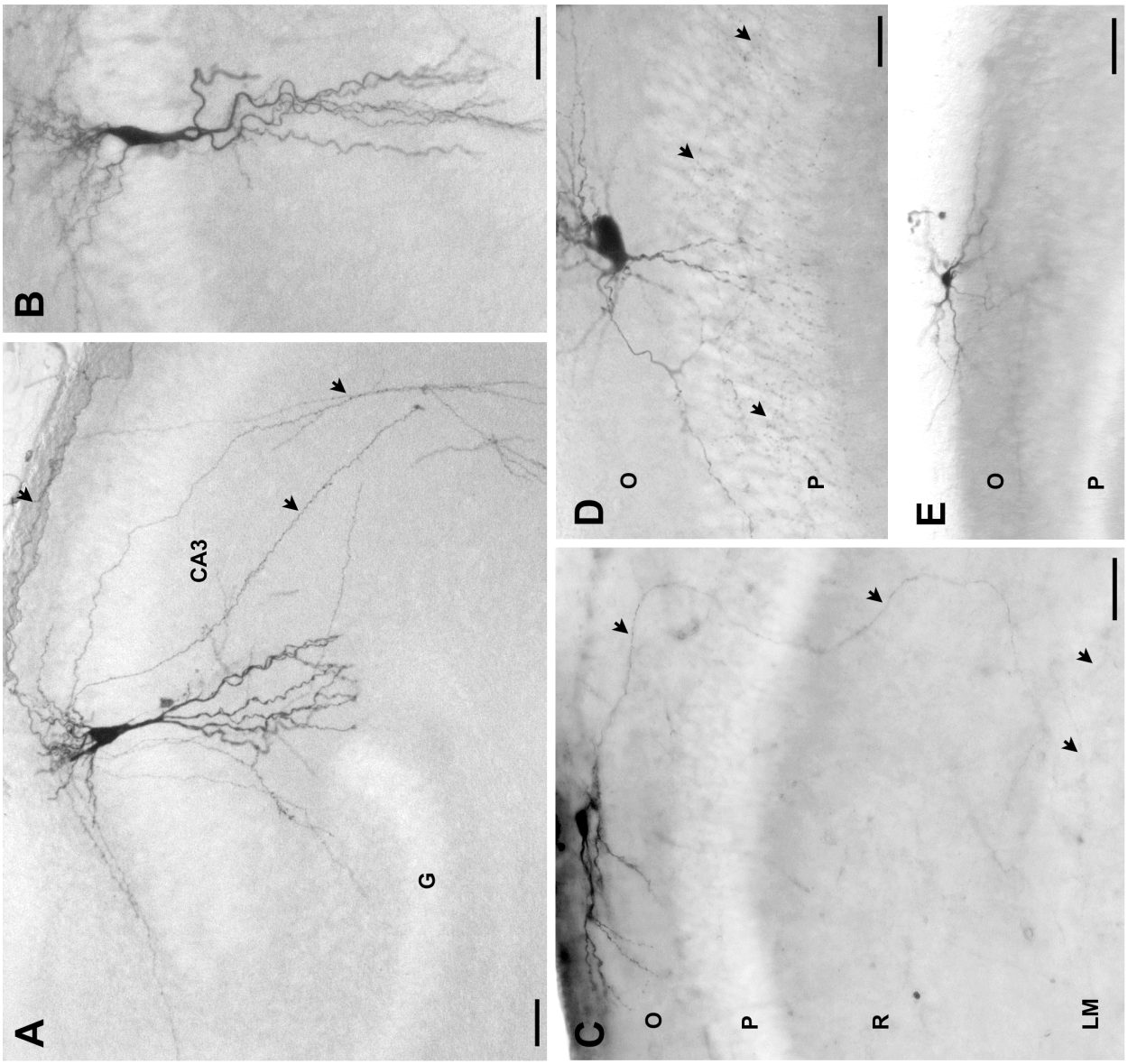
A
CA3
G
B
C
O
P
R
LM
D
O
P
E
O
P

Figure S3. HS cells depolarize their targets.

A. Example of a connection between two HS cells (HS1 and HS2) recorded in voltage clamp mode using a CsCl based intracellular solution in normal ACSF. A 5 ms long depolarization to -40 mV of the HS1 triggered an unclamped action potential. The action potential triggered an IPSC in the postsynaptic HS2 cell. This IPSC was blocked following the application of the $GABA_A$ receptor antagonist bicuculline (10 μM).

(B) Example of a connection between a HS cell and an O-LM interneuron recorded in current clamp mode using a K-gluconate based intracellular solution in normal ACSF. The HS and the O-LM cells were maintained at -60 mV and -80 mV, respectively. A 5 ms long, 400 pA current injection triggered an action potential in the HS cell, which produced a depolarizing IPSP in the postsynaptic O-LM interneuron. The neurotransmission was extremely reliable at these synapses. Each presynaptic cell was stimulated at least 100 times, for each connected pair. Neurotransmission failure was never encountered (not shown). The specific properties of these connections will be described in an independent study.

(C) Examples of the cell-attached patch-clamp recordings of the $GABA_A$ (*left panel*) and NMDA (*right panel*) receptor channels at different holding potentials in low Mg^{2+} ACSF.

(D) I-V relationships of the NMDA (circles) and $GABA_A$ (triangles) single channels permit to estimate resting membrane potential (Em) and the driving force of GABA mediated current (DF_{GABA}) in low Mg^{2+} ACSF. The holding potential value (Vp) at which the IV curve of NMDA currents crosses the x-axis corresponds to the resting membrane potential. The cross point of the GABA IV-curve and the x-axis gives a negative value for DF_{GABA}. In this example Em = -71.4mV, DF_{GABA} = -21.1 mV. The reversal potential for GABA currents is thus -50.3 mV in this HS cell.

(E1) Schematic view of the experimental protocol: A large GFP+ interneuron (putative HS cell) was stimulated locally. Putative targets were probed with a second electrode using the loose cell configuration.

(E2) A train of 10 action potentials at 100 Hz was evoked in the presynaptic cell and the presence of spikes in the postsynaptic cell detected. (a) In normal ACSF, the stimulation did not evoke a spike in the target. (b) After 3 ILEs in low Mg^{2+} ACSF, the same

stimulation protocol evoked spikes in the same postsynaptic cell. (c) The recording electrode was pulled back by 30 μm in low Mg^{2+}. No spike was detected, showing that they were generated by the neuron in loose cell configuration.

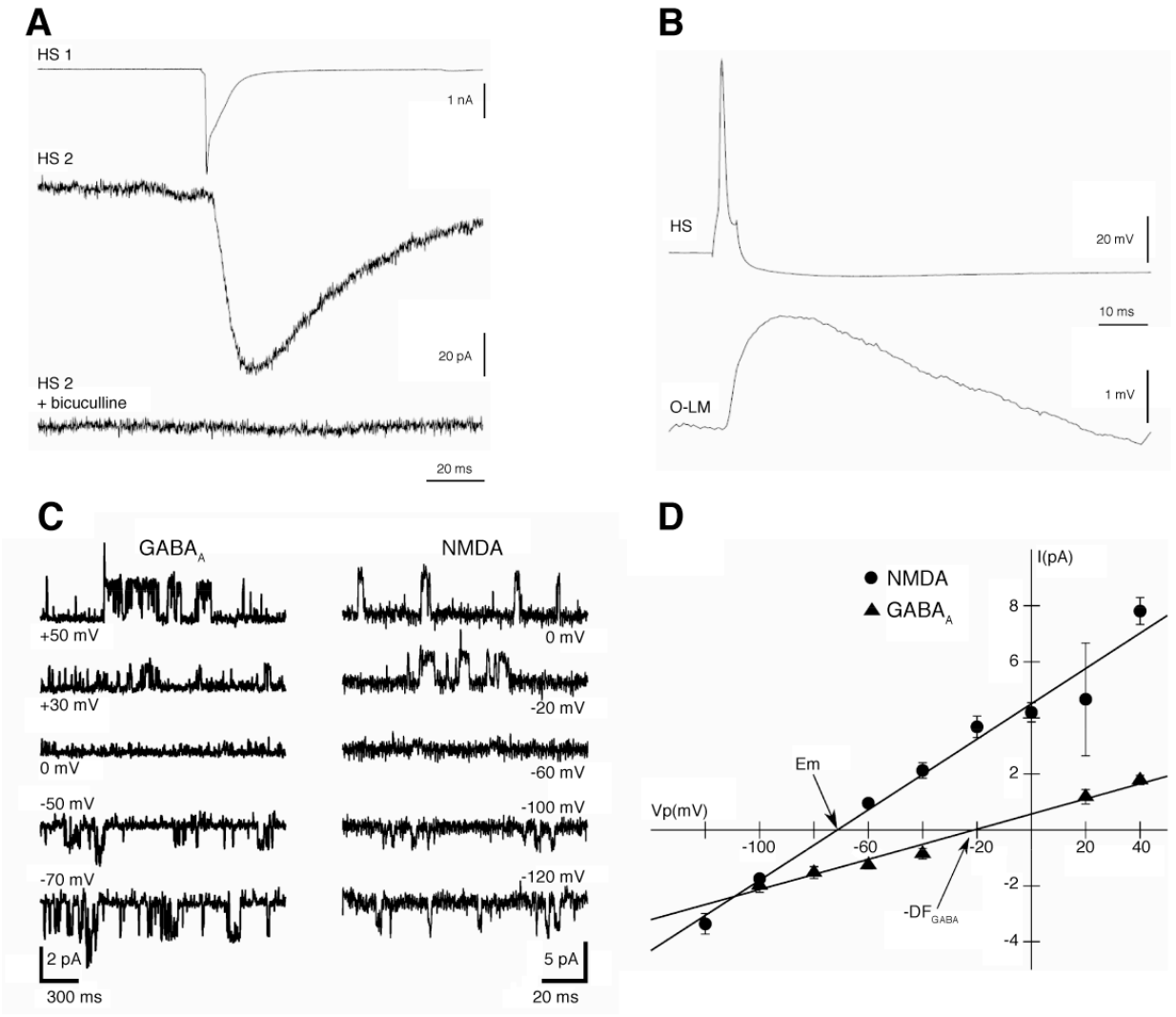
A
HS 1
1 nA
HS 2
20 pA
HS 2
+ bicuculline
20 ms
B
HS
20 mV
10 ms
O-LM
1 mV
C
GABA$_A$
NMDA
+50 mV
0 mV
+30 mV
-20 mV
0 mV
-60 mV
-50 mV
-100 mV
-70 mV
-120 mV
2 pA
300 ms
5 pA
20 ms
D
I(pA)
NMDA
GABA$_A$
8
6
2
-2
-4
Em
Vp(mV)
-100
-60
-20
20
40
-DF$_{GABA}$
E
1
2
a
b
c
50µV
100 ms

Figure S4. GFOs in GIN mice have similar properties to that found in rats.

(A) Comparison of immunohistochemical labeling for GFP and somatostatin in adjacent sections of a GIN-mouse septo-hippocampal formation (SHF) at P6. The SHF was used for electrophysiological recordings (control illumination configuration) prior to immunohistochemical processing.

(A1) Some GFP-containing neurons are observed in the *stratum oriens* (O) of CA1-3. *Top panel:* Many neurons are present in the subiculum whereas only few are observed in the hilus (H) of the dentate gyrus (DG). *Bottom panel:* Higher magnification of CA1 stratum oriens showing one GFP-containing neuron with a horizontal dendritic arborization.

(A2) Numerous somatostatin-containing neurons are present in the *stratum oriens* of CA1-3 and in the subiculum. *Top panel:* Many neurons are also observed in the hilus of the dentate gyrus. *Bottom panel:* Higher magnification of the CA1 *stratum oriens*, showing that the number of somatostatin-containing neurons is about ten times higher than that of GFP-containing neurons in this region (compare *bottom panels* in A1 and A2). This result is similar to that found in adult GIN-mice, in which nearly 100% of GFP-containing neurons in the hippocampal formation are GABAergic and contain somatostatin, whilst 15% of somatostatin-containing interneurons in the *stratum oriens* of CA1 contain GFP (Oliva et al., 2000).

(A3) Many GFP-containing neurons in the *stratum oriens* display morphological features of HS neurons.

Scale bars: A1-A2 *top panels* and A3 = 100 mm; A1-A2 *bottom panels* = 25 mm.

O. *stratum oriens*, P: *stratum pyramidale*, R: *stratum radiatum*, LM: *stratum lacunosum moleculare*.

(B) Under low Mg^{2+} conditions, ILEs and GFOs recorded in GIN mice SHFs were similar to those recorded in rats and in normal mice. GFOs were present at the onset of the ILE. The CA1 pyramidal cell (Pyr CA1) remained silent, whilst simultaneously recorded HS neurons (HS1 and HS2) fired at high frequency before the occurrence of field GFOs. Two interneurons were simultaneously recorded in voltage-clamp mode in a different experiment (IN V-clamp). The traces were aligned of the field GFOs (not shown).

GABAergic inputs, displaying a gradual build-up, arrived before field GFOs, consistent with the early firing of HS neurons. Glutamatergic inputs arrived after the initiation of the GFOs. Similar results were found in 5 CA1 pyramidal cells (n = 5, all silent), HS neurons (n=23) and interneurons (n=34).

(C) Under high K^+ conditions, ILEs and GFOs recorded in GIN mice SHFs were similar to those recorded in rats and in GIN mice. GFOs were present at the onset of the ILE (*top panel*): (C1) The HS neurons fired at high frequency before the occurrence of the GFOs (n=7) whereas (C2) the O-LM interneuron fired during the GFOs (n=4).

(D) Triggered with kainic acid, ILEs and GFOs recorded in GIN mice SHFs were also similar. GFOs were present at the onset of the ILE (*top panel*): (D1) The HS cells fired at high frequency before the occurrence of GFOs (n=4) and (D2) the O-LM interneuron fired during GFOs (n=4 interneurons). Similar findings were obtained with 4AP (n=3, not shown).

E. Relationship between HS (E1) and non-HS (E2) neurons firing frequency and GFOs frequency in kainic acid, 4AP or high K^+ conditions. The firing frequency of non-HS GABAergic neurons during GFOs is similar to the field GFO frequency. In contrast, the firing rate of HS cells before GFOs is on average higher than the GFOs mean frequency.

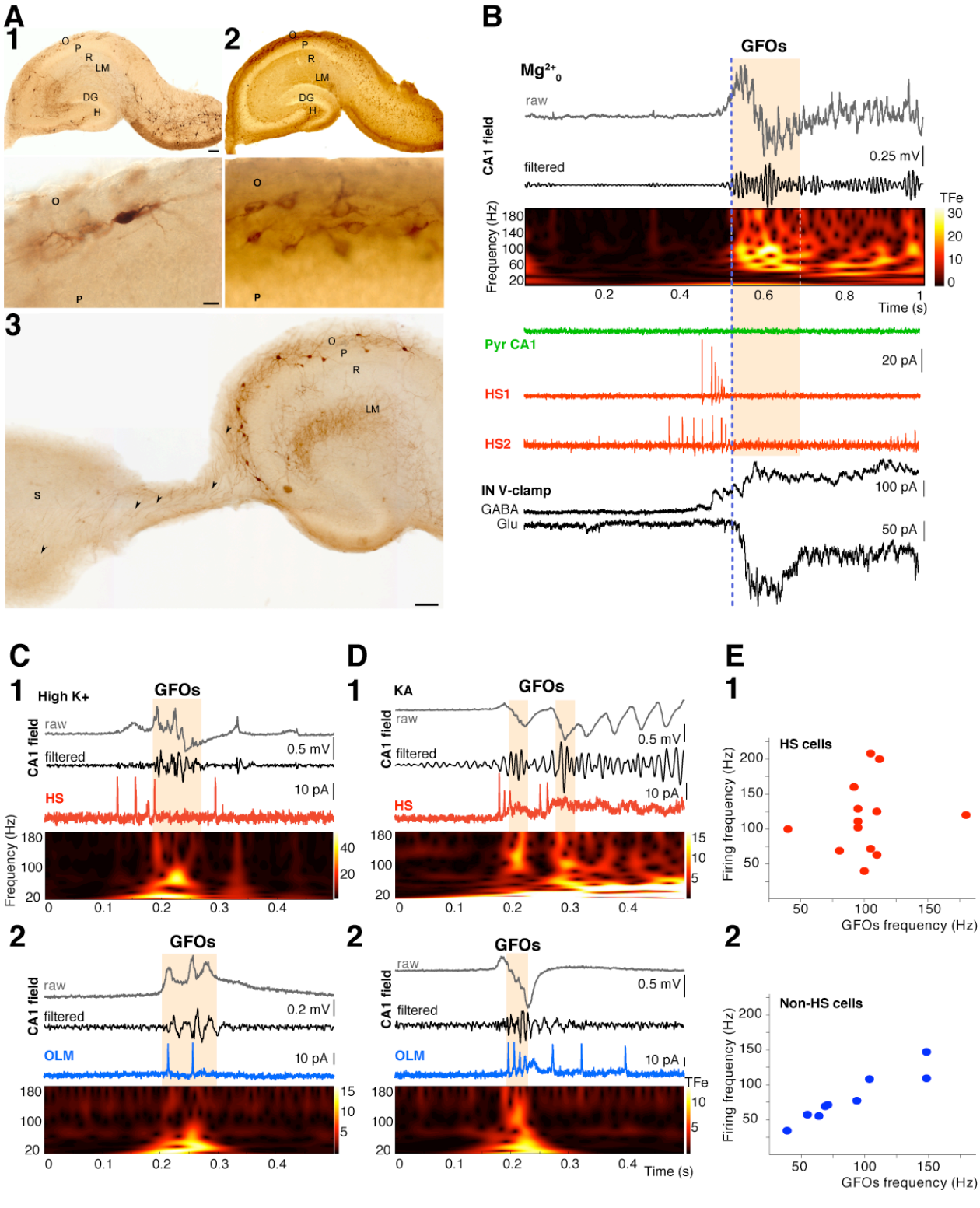
A
1
O
P
R
LM
DG
H
2
3
S
B
GFOs
Mg2+0
raw
filtered
CA1 field
0.25 mV
TFe
Frequency (Hz)
180
140
100
60
20
30
20
10
0
0.2
0.4
0.6
0.8
1
Time (s)
Pyr CA1
20 pA
HS1
HS2
IN V-clamp
GABA
Glu
100 pA
50 pA
C
1
High K+
GFOs
0.5 mV
10 pA
HS
40
2
0.2 mV
OLM
15
10
5
D
KA
TFe
Time (s)
E
HS cells
Firing frequency (Hz)
GFOs frequency (Hz)
Non-HS cells

Supplemental Experimental Procedures

The intact septo-hippocampal formation (SHF)

All protocols were designed according to Inserm guidelines for the care and use of animals. Experiments were performed on intact SHFs taken from Wistar rats between postnatal day (day of birth) P5 and P7. Animals were killed and brains were extracted from the skull at 4°C. The two hemispheres were separated and dissected in order to obtain SHFs. They contained the hippocampal formation, the septum and parts of adjacent neocortical areas. The same procedure was applied for the experiments performed in GIN (GFP-expressing Inhibitory Neurons) mice intact SHFs. Each SHF was placed in oxygenated (95% O_2 and 5% CO_2) ACSF with the following composition (in mM): NaCl, 126; KCl, 3.5; $CaCl_2$, 2; $MgCl_2$, 1.3; $NaHCO_3$, 25; $NaHPO_4$, 1.2; glucose 10 (pH 7.3). After at least 1 h rest at room temperature, SHFs were transferred to the recording chamber where they were fully submerged and superfused with ACSF oxygenated at 32.0 ± 0.5°C at a flow rate of 7.0±0.2 mL/min. After 30 min, SHFs were then superfused with an ACSF without magnesium ions (low Mg ACSF). For some experiments (see Figure S4C-D), the epileptiform activity was generated by the addition of 300 nM of Kanic Acid in the ACSF or by the addition of 5mM of KCl in the ACSF.

Electrophysiological recordings

Field recordings were performed with extracellular microelectrodes filled with ACSF, usually placed in the *stratum oriens* of the CA1 area of the hippocampus. Simultaneously with field recordings, individual cells were recorded using patch-clamp techniques in cell-attached and whole-cell configurations. Interneurons and pyramidal cells were blindly recorded, or were identified using IR-DIC microscopy or a combination of fluorescence/IR-DIC for GIN mice through a 60x water immersion objective. Microelectrodes had a resistance of 4–8 MΩ, and internal solution of the following composition was used to record EPSCs and IPSCs (in mM): 135 Cs-gluconate, 2 $MgCl_2$, 0.1 $CaCl_2$, 1 EGTA, 2 MgATP, 0.5 Na_4GTP, 10 HEPES, 0.5% biocytin (pH 7.3; 270-280 mOsm). Access resistance was monitored throughout the experiments (range 12-30

MΩ). Experiments were discarded if series resistance increased by more than 20%. Cells were kept at -60 mV or +10 mV for the analysis of glutamatergic (NMDA and AMPA receptor-mediated currents) or GABAergic spontaneous postsynaptic currents, respectively. These currents were blocked by D-APV/NBQX and bicuculline, antagonists of NMDA/AMPA and $GABA_A$ receptors respectively (not shown). All data were acquired using an analogic-digital converter (Digidata 1322B Axon Instruments, CA, USA) and analyzed using Clampfit (Axon laboratories, CA, USA) or Matlab based software. During recordings, all neurons were passively filled with biocytin for *post hoc* morphological identification.

Measurement of membrane potential and reversal potential of $GABA_A$ receptor-mediated currents

Procedures are previously described in (Tyzio et al., 2003). Interneurons were first recorded in the cell-attached configuration, with a pipette solution containing nominally Mg^{2+}-free ACSF with NMDA (10 μm), glycine (1 μm), strychnine (1 μm) and biocytin (0.5%). The holding potential was varied to obtain IV curves of single NMDA channels. The potential at which NMDA receptor-mediated currents reverse corresponds to the cell resting membrane potential. The pipette was then gently removed and the same neuron re-patched in the cell configuration using an internal solution of the following composition (in mM): NaCl, 120; tetraethylammonium–Cl, 20; KCl, 5; 4-aminopyridine; 5; $CaCl_2$, 0.1; $MgCl_2$, 10; glucose, 10; GABA, 0.005; Hepes–NaOH, 10; 0.5% biocytin (pH 7.3). The holding potential was varied to obtain IV curves of single $GABA_A$ receptor-mediated currents and to define the reversal potential of $GABA_A$ receptor-mediated currents. At the end of the recording, the patch was ruptured to allow biocytin to diffuse during 20 min to enable *post hoc* morphological identification of the recorded interneurons.

Connected interneuron pairs

To test for synaptic connections between neuron pairs recorded in voltage clamp mode with the Cs-gluconate based internal solution described above, one cell was briefly (5 ms) depolarized to -40 mV to produce a voltage-escape action potential. The synaptic

connection was assessed by the presence of a postsynaptic current in the second cell with a fixed latency, paired pulse depression/facilitation, a reversal potential in keeping with the composition of the intracellular solution (-60 mV for GABAergic currents), and its sensitivity to the $GABA_A$ receptor antagonist bicuculline (10 μM).

To establish the connectivity pattern of HS cells, the internal solution of the following compositions were used (in mM): 150 CsCl, 4.6 $MgCl_2$, 0.1 CaI_2, 1 EGTA, 10 HEPES, 4 Na-ATP, 0.4 Na-GTP, 0.5% biocytin, pH 7.3, osmoloratity 260-290 mOsm (for voltage clamp recordings); and 90 K-gluconate, 40 CsCl, 1.2 NaCl, 3.5 KCl, 1.7 $MgCl_2$, 0.05 EGTA, 10 HEPES, 2 Na-ATP, 0.4 Na-GTP, 10 creatine-phosphate, 0.5% biocytin, pH 7.3, osmoloratity 260-290 mOsm (for current clamp recordings). The holding potential was kept at -60 mV in voltage clamp mode (CsCl based solution), giving rise to inward GABAergic currents in the postsynaptic cells. Presynaptic cells were voltage-clamped at -60 mV, and unclamped action potentials were triggered by 5 ms depolarizations to -20 mV. In current-clamp mode (K-gluconate based solution), the membrane potential of the postsynaptic cell was kept at -80 mV with constant current injection, giving rise to depolarizing GABAergic postsynaptic potentials. The presynaptic cell was kept at -60 mV and injecting 5 ms depolarizing pulses (400-600 pA) evoked action potentials. Presynaptic interneurons were stimulated every 8 s. Prior recordings, cells with a large multipolar soma close to the *stratum oriens* surface were selected under visual control. This selection procedure led to 1/3 probability to find a synaptic connection between two cells.

Pharmacological experiments

They were performed as previously described (Quilichini et al., 2002). Briefly, after the induction of 3 network discharges, the drug solution was applied for 30-60 min. GFOs were determined (see below) at the onset of the 3 initial ILEs (control) and at the onset of ILEs occurring during drug application.

Histochemical Methods

All SHFs processed for the detection of biocytin-filled neurons or for the green fluorescent Protein (GFP) and somatostatin immunohistochemical labeling were fixed immediately after electrophysiological recordings in a solution of 4% paraformaldehyde in 0.12 M phosphate buffer (PB, pH 7.4) overnight at 4°C. After fixation they were rinsed in PB for 1.5 hr, cryoprotected in a 20 % sucrose solution overnight at 4°C and quickly freeze-thaw in liquid nitrogen. SHFs were cut in a transverse plane on a vibratome and 150 μm thick sections were collected sequentially in PB.

Detection of biocytin-filled neurons was performed for each SHF, processing all adjacent sections collected from the whole structures as followed. Sections were pretreated for 30 min in 1% H_2O_2 prepared in PB to neutralize endogenous peroxidases, rinsed in a potassium phosphate-buffered saline (0.02 M KPBS, pH 7.4) and incubated overnight in 1:100 avidin-biotinylated horseradish peroxidase complex (Vestastain ABC Peroxidase kit, Vector laboratories, Burlingame, CA) diluted in KPBS containing 0.3 % Triton X-100. After 1 hr rinses in KPBS, sections were then processed for 15 min with 0.06% 3,3'-diaminobenzidine tetrahydrochloride (DAB, Sigma, France) and 0.01% H_2O_2 diluted in KPBS, rinsed in KPBS, mounted on Superfrost plus slides and cover-slipped in an aqueous mounting medium (Crystal/Mount, Biomeda, Foster City, CA). Biocytin-labeled interneurons were identified and their complete dendritic and axonal arborisations were reconstructed from serial adjacent sections with the NeuroLucida system (Microbrightfield, Colchester, VT).

Immunohistochemical labeling for GFP and somatostatin was performed in 8 SHFs. For each SHF, two adjacent sections, every three sections, were selected through the entire structures. One section was processed for the immunodetection of GFP, the other one for the detection of somatostatin as followed. Sections were pretreated for 30 min in 1% H_2O_2 prepared in PB to neutralize endogenous peroxidases and rinsed for 1.5 hr in 0.02 M KPBS. Then, sections were pre-incubated for 1 hour at room temperature (RT) in KPBS containing 0.3% Triton X-100, 3% normal goat serum (NGS, Vector) and incubated overnight at RT in a polyclonal antiserum directed against GFP (rabbit anti-GFP, IgG fraction, A11122; Molecular Probes, Eugene, OR; 1:3000) or a polyclonal somatostatin-antiserum raised in rabbit (IHC 8001, Peninsula Laboratories,

Belmont, CA; 1:4000) diluted in KPBS containing 0.3% Triton X-100, 1% NGS. After these steps, sections were rinsed in KPBS, incubated for 1 hr at RT in biotinylated goat anti-rabbit immunoglobulin G (Vector) diluted 1:200 in KPBS containing 3% NGS; rinsed in the same buffer and incubated for 1 hour at RT with avidin-biotinylated horseradish peroxidase complex (Vector) diluted 1:100 in KPBS. After 1 hr rinses in KPBS, sections were processed for 15 min with 0.06% 3,3'-diaminobenzidine tetrahydrochloride (DAB, Sigma, France) and 0.01% H_2O_2 diluted in KPBS. The sections were then rinsed in KPBS, mounted on Superfrost plus slides, dried, dehydrated, and coverslipped with permount (Fisher Scientific, Washington, PA).

Drugs

Bicuculline methochloride, 2,3-dioxo-6-nitro-1,2,3,4-tetrahydrobenzo[f] quinoxaline-7-sulfonamide (NBQX) and kanic acid were purchased from Tocris Cookson Ltd (UK). Drugs were first dissolved in water or in DMSO and then diluted in ACSF. The final concentration of 0.1% DMSO has no effect on network activity.

Gamma-frequency oscillations analysis

A wavelet time-frequency (TF) analysis was used to analyze to determine precisely the mean frequency, the beginning and the duration of the field GFOs. The advantage of the wavelet analysis lies in the fact that the time resolution is variable with frequency, so that high frequencies have a sharper time resolution (Le Van Quyen and Bragin, 2007; Torrence and Compo, 1998). The Gabor wavelet is applied and uses a wave-like scalable function that is well localized in both time and frequency:

$$\Psi_{\tau,f}(u) = \sqrt{f}\,\exp(\,j2\pi f(u-\tau))\exp\left(-\frac{(u-\tau)^2}{\sigma^2}\right).$$

This wavelet represents the product of a sinusoidal wave at frequency *f*, with a Gaussian function centered at time t, with a standard deviation s proportional to the inverse of *f*. The wavelet coefficients of a signal *x(t)* as a function of time (t) and frequency (f) are defined as: $W(\tau, f) = \int_{-\infty}^{+\infty} x(u)\Psi_{\tau,f}(u)du$. It depends solely on s, which sets the number

of cycles of the wavelet: *nco*= 6*f*s. This value *nco* determines the frequency resolution of the analysis by setting the width of the frequency interval for which phase are measured. We chose *nco=5*.

As a criterion of the significance for the TF representations, we required that the TF peak energy to exceed the mean + 3 standard deviation of a baseline taken far away from synchronized events. Thus, by using the background signal in the same way at each frequency, the method allowed to statistically control the levels of oscillatory activity from that one would expect by chance and fairly compare oscillatory episodes across frequencies. To detect oscillatory events, we designed an algorithm to identify the periods within the signal that exhibits high-power oscillatory activity at a particular frequency, lasting a few cycles. We defined oscillatory events by detecting local maxima in the normalized TF representations with duration longer than *K* cycles at a particular frequency, during which the power exceeded *N* standard deviations of baseline. We have adjusted the thresholds (*K*,*N*) to be relatively insensitive to sharp transients. The duration threshold was set to 5 cycles (i.e. *5/f* sec) and the amplitude threshold was set to 3 standard deviations.

Phase-locking between two field oscillations

We used the procedure described in (Lachaux et al., 1999) to overcome some limitations of conventional methods which cannot disentangle instantaneous amplitudes and phases (see (Le Van Quyen et al., 2001) for details). The important advantage of this method is that the phase components can be analyzed separately from the amplitude components, which can be quite noisy or even non-correlated (Le Van Quyen and Bragin, 2007). Two steps are used: 1) *Estimation of the phase*: The first step is to measure the instantaneous phase-difference between signals around the frequency of interest. The phase of the signals are extracted from the coefficients of their wavelet transform at the target frequency between 60 and 200 Hz. These coefficients are the result of a convolution of the original signal with a complex Gabor wavelet (see previous section). 2) *Quantification of the degree of phase locking*: The phase-difference between

the signals x and y at frequency f and time t can be derived from the angles of their wavelet-coefficients:

$$\exp(\ j(\phi_y(f,\tau) - \phi_x(f,\tau))) = \frac{W_x(\tau,f)W^*y(\tau,f)}{|W_x(\tau,f)||W_y(\tau,f)|}$$

A phase Locking value (PLV) is then defined as:

$$PLV\ (f,t) = \left| \frac{1}{\delta} \int_{t-\delta/2}^{t+\delta/2} \exp(\ j(\phi_y(f,\tau) - \phi_x(f,\tau)))\, d\tau \right|$$

PLV depends then on two parameters: *nco* (see previous section) and the size d of the window of temporal integration, which can be expressed in a number of cycles at a chosen frequency *f*: *ncy* =*f*.d. In this sense, *ncy* determines the temporal resolution of the analysis where the synchrony estimation remains stable. We usually chose *ncy* between 6 and 10. PLV ranges from 0 to 1 with 1 indicating the strongest phase-locking. The significance of each PLV is estimated via a comparison with a distribution PLV obtained between independent Gaussian signals (100 pairs) with same duration as the original signals are generated. For each of them, the maximum PLV is measured to build a distribution of 100 values. A significant synchrony is detected when less than 1% of the surrogate values were greater than the original PLV (Le Van Quyen et al., 2001).

Phase-locking between spikes and field oscillations

We used the procedure described in (Jacobs et al., 2007) which characterizes the phase distribution of the field oscillations at the moment of the spike onset. If the firing of a given neuron is independent of the field oscillation, the distribution of its phase values will be random. Conversely, if the firing of a given neuron is phase-locked to the field oscillation, its phase value distribution will be unimodal. Following this strategy, oscillatory phase and power of the field potential was computed using Gabor wavelets (*nco=5*) at frequencies between 20 and 200 Hz (see previous paragraphs). We considered a neuron phase-locked at a particular frequency if the hypothesis of circular uniformity for its field phase distribution could be rejected at $P < 0.001$ using a Bonferroni-corrected Rayleigh test (Fisher, 1993). Briefly, given *n* phase values f_i define

the first trigonometric moment $m = (1/n) \sum_1^n e^{j\phi i}$. The sample mean direction or preferred phase μ is given by the orientation of *m*, while the mean resultant value R is given by the modulus of *m*. The Rayleigh statistic is $Z = n R^2$, and the probability that the null hypothesis of sample uniformity holds is given by $P = e^{-Z} [1 + (2Z - Z^2)/(4n) - (24Z - 132Z^2 + 76Z^3 - 9Z^4)/(288n^2)]$. For $n > 50$, the approximation $P = e^{-Z}$ is adequate (Fisher, 1993; Siapas et al., 2005).

Instantaneous frequency of spike and post-synaptic current

Spikes were detected in cell-attached recordings using a threshold detection algorithm (>4:1 signal to noise ratio). The instantaneous spike frequency was measured by convolving the timing of each detected event with a Gaussian function of variable standard deviation (Szucs, 1998). Post-synaptic current (PSC) were counted individually in whole-cell recordings if their peak height was greater than the half-peak amplitude of the background activity. The instantaneous PSC frequency was measured by convolving the timing of each detected event with a Gaussian function of a standard deviation of 10 ms.

Ablation of GFP-containing interneurons

After recording several GFOs in GIN mice, the region around the recording electrode was scanned under visual control and florescence illumination, until a GFP interneuron in *stratum oriens* close to the surface (where most HS cells are located) was found. The region remained illuminated during 5 min. Under a 60x Olympus objective on a Zeiss FSII microscope and with maximum power illumination (Zeiss), this duration was found to be optimal for all fluorescence to disappear in the field. Before the continuous illumination, the soma of GFP-containing (fluorescent) neurons was also easily identifiable under IR. Following focused illumination, the soma was no longer observed (neither the nucleus, nor a “phantom cell” could be seen), neither under fluorescence illumination nor IR. However, GFP-negative interneurons could still be visible under IR in the illuminated field (not shown). Over-activation of GFP is deleterious, presumably via the production of free radicals. In these preparations, no biocytin-filled GFP-positive

neurons (n=5, recorded before illumination) were ever detected. However, in two SHFs, biocytin-filled axonal processes were observed in the septum, strongly suggesting that HS cells (n=2) were recorded and labeled before the illumination protocol (not shown). After checking the disappearance of the illuminated GFP-positive neurons, the field was moved to the next target GFP-positive neurons. The field was moved in an elongated spiral-like manner, centered on the extracellular recording electrode, with a predominant direction along the long, septo-temporal, axis of the hippocampus. In parallel to the illumination procedure, the presence of GFOs was checked online each time ILEs occurred. The illumination procedure was stopped when 3 successive ILEs did not display GFOs at their onset. Sham experiments were performed the contralateral SHFs recorded in the same conditions either illuminated and scanned under visible light with the 60X objective (n=3) or illuminated with fluorescence with a wide field 5X Zeiss objective (n=3). Sham illumination lasted one hour, exceeding by 15 min the longest duration of the focused illumination procedure. Immunohistochemical experiments for the detection of GFP were then performed in these preparations to assess the loss of GFP-immunolabeled neurons in the regions directly under illumination, or their survival in control experiments.

Elimination of GFP-negative interneurons in GIN mice

In order to destroy GFP-negative *stratum oriens* interneurons, we designed a double-barreled ACSF shotgun. Electrodes made of theta tubes were pulled with the parameters used for patch clamp electrodes. Both compartments were filled with ACSF. The electrode was inserted in a modified electrode holder. Two wires were introduced in each compartment, and connected to a stimulator. *Stratum oriens* GFP-negative interneurons were selected around the field electrode. The tips of the double-barreled electrode were apposed to the soma of the interneuron. The stimulus pulse ejected a "bullet" of ACSF (at an estimated maximum distance of 5 μm), which perforated the membrane, effectively killing the interneuron. The procedure was repeated by moving around the stimulating electrode. This type of stimulation was not sufficient to evoke a field response.

HS cells stimulation experiments

Putative HS cells were identified as GFP-positive neurons with large cell body located in the *stratum oriens*. The HS cell was stimulated with bipolar glass electrode 5-10mkm tip diameter pulled from theta glass tube (Warner instruments). To check the stimulation effectiveness, 200 μs (1/5s) stimuli were applied and a response of the stimulated neuron was recorded with a recording glass electrode (5-8 μm tip diameter) connected to the preamplifier of the Multiclamp 700b (current clamp mode). We used the loose patch configuration to test the result of the HS cell stimulation on neighboring neurons. To establish a contact with the target neuron, the recording electrode was approached to the cell body and a gentle suction was applied. The stimulus current intensity was adjusted to the minimal value sufficient to induce spiking in the stimulated neuron (50-170μA). Then 2-4 neurons surrounding stimulated one were tested for their ability to generate spikes in response to the high frequency stimulation (10 stimuli of 100Hz train) of the putative HS cell (Figure S3E1). Before ILEs induction, spikes never occurred in the 500ms time window after the stimulation onset (Figure S3E2a). After transition to low Mg^{2+} ACSF and the occurrence of 3 ILEs, the response on stimulation of the GFP-positive neuron was recorded in same neurons. To check that the detected spikes are indeed generated by the recorded cell, the stimulation was repeated after the recording electrode had been taken ~30 μm away from the recorded cell. As Figure S3E2c shows, no spike was detected in such configuration.

Supplemental references

Fisher, N. (1993). Statistical analysis of circular data (Cambridge: Cambridge University Press).

Jacobs, J., Kahana, M.J., Ekstrom, A.D., and Fried, I. (2007). Brain oscillations control timing of single-neuron activity in humans. J Neurosci *27*, 3839-3844.

Lachaux, J.P., Rodriguez, E., Martinerie, J., and Varela, F.J. (1999). Measuring phase synchrony in brain signals. Hum Brain Mapp *8*, 194-208.

Le Van Quyen, M., and Bragin, A. (2007). Analysis of dynamic brain oscillations: methodological advances. Trends Neurosci *30*, 365-373.

Le Van Quyen, M., Foucher, J., Lachaux, J., Rodriguez, E., Lutz, A., Martinerie, J., and Varela, F.J. (2001). Comparison of Hilbert transform and wavelet methods for the analysis of neuronal synchrony. J Neurosci Methods *111*, 83-98.

Oliva, A.A., Jr., Jiang, M., Lam, T., Smith, K.L., and Swann, J.W. (2000). Novel hippocampal interneuronal subtypes identified using transgenic mice that express green fluorescent protein in GABAergic interneurons. J Neurosci *20*, 3354-3368.

Quilichini, P.P., Diabira, D., Chiron, C., Ben Ari, Y., and Gozlan, H. (2002). Persistent epileptiform activity induced by low Mg2+ in intact immature brain structures. Eur.J Neurosci. *16*, 850-860.

Siapas, A.G., Lubenov, E.V., and Wilson, M.A. (2005). Prefrontal phase locking to hippocampal theta oscillations. Neuron *46*, 141-151.

Szucs, A. (1998). Applications of the spike density function in analysis of neuronal firing patterns. J Neurosci Methods *81*, 159-167.

Torrence, C., and Compo, G.P. (1998). A practical guide to wavelet analysis. Bulletin of the American Meteorological Society *79*, 61-78.

Tyzio, R., Ivanov, A., Bernard, C., Holmes, G.L., Ben Ari, Y., and Khazipov, R. (2003). Membrane potential of CA3 hippocampal pyramidal cells during postnatal development. Journal of Neurophysiology *90*, 2964-2972.